JGR Oceans

RESEARCH ARTICLE
10.1029/2022JC019134

Scale-Dependent Temperature-Salinity Compensation in Frontal Regions of the Taiwan Strait

Hongyang Lin[1], Siyu Xu[1], Zhiyu Liu[1], Jianyu Hu[1], Fangtao Zhang[1], and Zhiyong Cao[1]

[1]State Key Laboratory of Marine Environmental Science, Department of Physical Oceanography, College of Ocean and Earth Sciences, Xiamen University, Xiamen, China

Key Points:

- In winter and spring, two slanted density fronts are formed in the Taiwan Strait with a cone-shaped isopycnal distribution
- Temperature and salinity are more (less) compensated from O(10 km) to O(1 km) scale in salinity-dominated (temperature-dominated) region
- The observed scale-dependent density compensation features can both be interpreted by the restratification-cooling mechanism

Correspondence to:
Z. Liu and J. Hu,
zyliu@xmu.edu.cn;
hujy@xmu.edu.cn

Citation:
Lin, H., Xu, S., Liu, Z., Hu, J., Zhang, F., & Cao, Z. (2023). Scale-dependent temperature-salinity compensation in frontal regions of the Taiwan Strait. *Journal of Geophysical Research: Oceans*, *128*, e2022JC019134. https://doi.org/10.1029/2022JC019134

Received 28 JUL 2022
Accepted 17 JAN 2023

Abstract Based on high-resolution, cross-frontal towed measurements, this study investigates temperature-salinity (T-S) compensation and its scale dependence in the Taiwan Strait. In winter and spring when the northeasterly monsoon is prevailing, colder and fresher waters flow southward along the coast of the Chinese mainland, which encounter the northward-flowing, warmer and saltier waters in the Taiwan Strait. Two slanted density fronts are generated across the interfacing zone forming a cone-shaped isopycnal distribution in the cross-frontal direction. Analyses based on the density ratio and Turner angle suggest the expected S-dominated and T-dominated types of density variations at the western and eastern density fronts, respectively. Exact T-S compensation is observed within the interfacing zone. Analysis of the scale dependence indicates that temperature and salinity get more (less) compensated from O(10 km) to O(1 km) scale in the S-dominated (T-dominated) frontal zone. Although contrasting density compensating features are observed on the two flanks of the transition zone, they can both be interpreted by the restratification-cooling mechanism. Specifically, the overturning cells due to submesoscale instabilities in the upper mixed layer slump isopycnals in the frontal zone, inducing shoaling of the mixed layer at both ends of the sampled sections. Surface cooling results in larger temperature drops in the shallower mixed layers, and thus increases (decreases) the degree of T-S compensation in the S-dominated (T-dominated) frontal zone at the scale for submesoscale instabilities to develop.

Plain Language Summary Variations of seawater density are determined mainly by temperature variations (T-dominated) in most of the global ocean, whereas salinity variations dominate in regions that are strongly influenced by river runoff or precipitation (S-dominated). The phenomenon that temperature and salinity having opposing effect on density is referred to as temperature-salinity (T-S) compensation. Using high-resolution field measurements, this study investigates the T-S compensation and its dependence on spatial scales in frontal regions of the Taiwan Strait. A prominent T/S front was observed in the Taiwan Strait in winter and spring, with S-dominated type of coastal waters on the mainland side and T-dominated type of waters in the central strait. There was no density front co-located with the T/S front due to T-S compensation; instead, there were two slanted density fronts located at different sides of the T/S front. Further analysis suggests that the degree of T-S compensation increases (decreases) with decreasing spatial scale in the western S-dominated (eastern T-dominated) front, which can be explained by the proposed restratification-cooling mechanism. Specifically, submesoscale instabilities induce secondary circulations which generate a shallower mixed layer at the west (east) end of the western (eastern) front, leading to a larger temperature reduction under surface cooling conditions.

1. Introduction

The density of seawater under a given pressure is jointly determined by its temperature and salinity. In most regions of the world ocean, density gradients are governed primarily by variations in temperature (T-dominated). In regions that are strongly influenced by river runoff or precipitation or regions with nearly constant temperature (e.g., surface polar areas), salinity changes would mainly govern density gradients (S-dominated). The density ratio, defined as the ratio of variations in density contributed by temperature to those contributed by salinity, is often used to quantify the relative effect of temperature and salinity on density. A special case occurs when temperature and salinity exactly cancel their respective effect on density, which has a density ratio of unity and is referred to as exact density compensation. This is in fact commonly observed at ocean fronts with colder and fresher water on one side and warmer and saltier water on the other. A consequence of the temperature-salinity (T-S) compensation is that strong fronts of temperature or salinity might end up with inconspicuous density

gradients. Strong sea surface density fronts are characterized by nearly vertical isopycnals which transfer their available potential energy to kinetic energy when slumping; the mixed-layer instabilities induce an overturning cell with positive (upward) buoyancy flux which restratifies the mixed layer, accompanied by active submesoscale processes (McWilliams, 2016). As revealed by nowadays high-resolution satellite images, the world oceans are characterized by prominent fine-scale sea surface temperature (SST) gradients corresponding to vigorous submesoscale structures (with conspicuous density fronts), due to the prevalence of T-dominated density variations.

T-S compensation has long been documented for major fronts in the North Pacific on both meso- and large scales (e.g., Roden, 1975). According to high-resolution towed measurements, exact T-S compensation was identified at all observed scales down to tens of meters in the mixed layer of North Pacific (Ferrari & Rudnick, 2000; Rudnick & Ferrari, 1999); below the mixed layer, the horizontal temperature gradients are partially compensated by salinity gradients with a density ratio of 2 (Ferrari & Rudnick, 2000). Such a depth-dependent compensation feature was later found to be also prevailing in the North Atlantic and Arabian Sea (Rudnick & Martin, 2002). In the Arctic Ocean, nonetheless, the temperature of the winter surface layer is very low (close to freezing) and almost constant, the surface mixed layer is found to be generally non-compensating with salinity dominating density changes (Timmermans & Winsor, 2013). Based on towed measurements, Spiro Jaeger and Mahadevan (2018) find that the surface mixed layer is also non-compensating in the Bay of Bengal that is strongly influenced by monsoonal precipitation and runoff, but more interestingly, that temperature and salinity get more compensated with decreasing spatial scales with a density ratio of unity (i.e., exact compensation) at O(1 km). They suggest that the submesoscale-selective compensation at salinity-fronts in this region is because surface cooling leads to a greater temperature drop on the shallower and less salty side of the front.

Previous studies examine T-S compensation in either T-dominated or S-dominated regions, with compensating features yet to be revealed in confluent regions with both types of density distribution. In winter and spring, a coastal current flows south-southwestward along the coast of the Chinese mainland (Hu et al., 2010). This flow, termed as Zhe-Min Coastal Current or simply China Coastal Current in the literature, carries relatively cold and fresh waters owing to its origin of the Changjiang River estuary. During the southward migration, the waters interface with the relatively warm and salty waters in the central Taiwan Strait. The latter waters are carried by a northeastward-flowing current regarded as an extension of the South China Sea Warm Current (Hu et al., 2010). The confluence of the two waters carried by the currents with reversing directions forms prominent fronts of temperature and salinity in the Taiwan Strait. Salinity changes are expected to dominate density variations for the waters on the mainland side, whereas the South China Sea Warm Current extension originates from the subtropical deep ocean and is expected to carry T-dominated waters. Based on high-resolution towed measurements, this study seeks to examine T-S compensation across the frontal areas in the Taiwan Strait for waters from contrasting regimes, and to further explore the scale dependence of the compensation.

2. Data and Methods

The towed measurements, satellite products and the defined quantities used for T-S compensation analysis are introduced below.

2.1. Towed Measurements

In March 2019, a process-oriented field campaign was carried out to conduct high-resolution cross-frontal measurements in the Taiwan Strait. Several cross-frontal sections were targeted according to the near-real time satellite SST images (Figure 1). Towed measurements of temperature and salinity were collected using the Acrobat LTV-50X vehicle (Sea Science Inc.), and underway velocities were simultaneously collected by a shipboard acoustic Doppler current profiler (ADCP). Considering the data completeness and quality, two cross-frontal sections of the towed measurements are used for further analysis (sections AB and CD in Figure 1). It is clear from Figure 1 that sections AB and CD traverse the along-strait front with the largest temperature gradient. The Acrobat vehicle goes up and down collecting data in profiles with a yo-yo shape. The raw towed profiles have a horizontal interval ranging from 300 to 700 m with an average of about 500 m; the vertical spacing of the towed measurements is relatively large (small) in the descending (ascending) profiles, but overall with a mean (root mean square) of 0.4 m (0.6 m). For analysis, the raw measurements are interpolated to regular bins with a

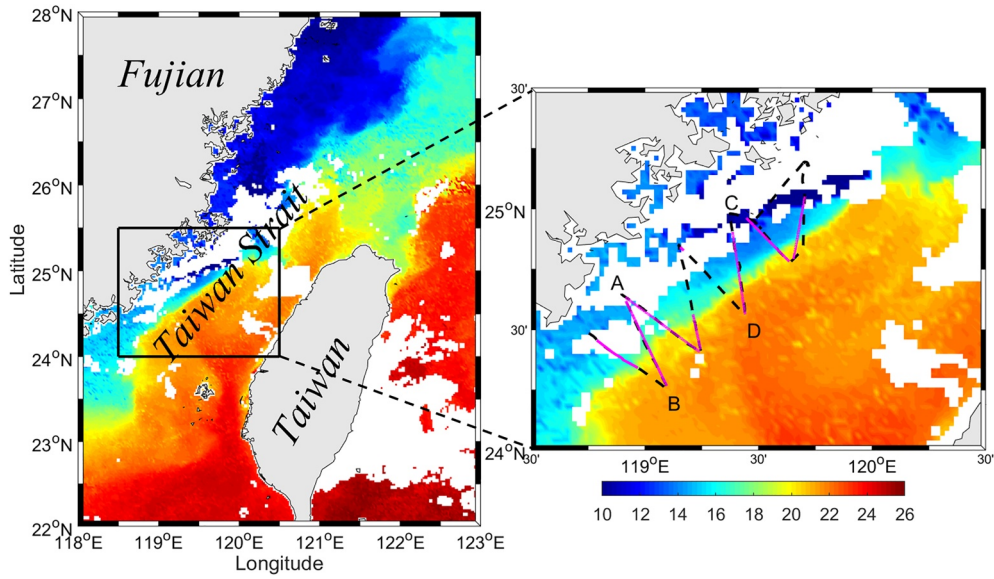

Figure 1. (Left) Map of the Himawari 8-based sea surface temperature (SST) (in °C) on 10–11 March 2019 in the vicinity of Taiwan Strait. (Right) Zoom-in version of SST in the Taiwan Strait superimposed with the ship trajectories (black dashed lines) and locations where towed measurements were conducted (magenta lines).

horizontal grid spacing of 100 m and a vertical interval of 0.5 m from 5 to ~50 m depth (Figure 2). The underway velocities have spatial resolutions of ~270 m in the horizontal and 1 m in the vertical. The towed measurements were conducted from 08:58 a.m., 10 March to 02:58 a.m., 12 March 2019 (UTC), but the time span for the measurements across either section AB or CD is ~3.5 hr, which is about a quarter of the tidal period in the study region (primarily semidiurnal tide). Hence tides are not expected to contaminate sectional structures of the thermohaline properties observed by the towed measurements.

2.2. Satellite and Reanalysis Data

In addition to the field measurements, a set of satellite and reanalysis products are also used. The Himawari 8 is a geostationary satellite providing snapshots with a spatial resolution of 2 km. Its daily-averaged SST product, distributed by the Japan Aerospace Exploration Agency, is used in this study. The mean surface ocean currents are

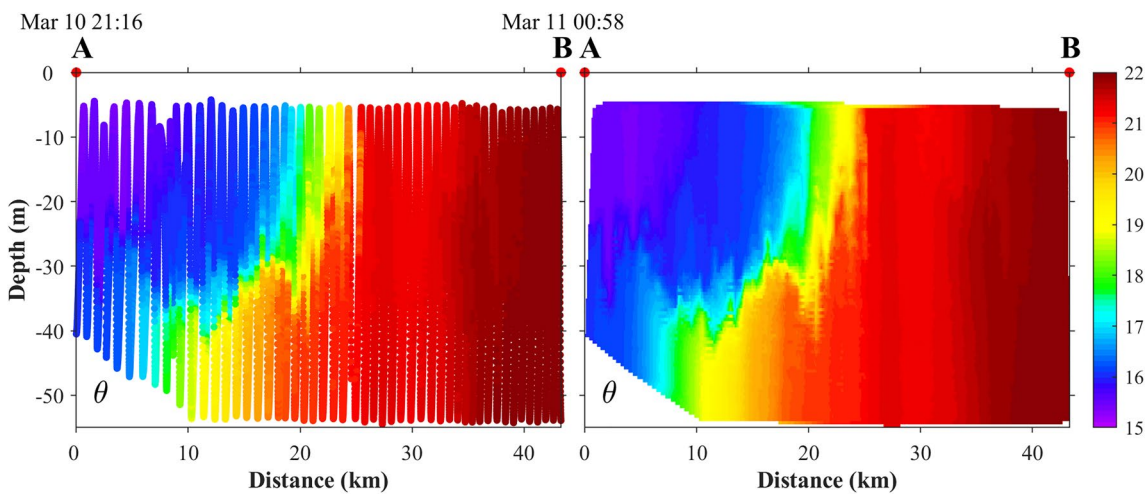

Figure 2. (Left) Raw Acrobat measurements of potential temperature from section AB. The spatial interval between each profile is about 500 m. (Right) The interpolated, gridded potential temperature based on the raw measurements. The interpolated data have a horizontal grid spacing of 100 m and a vertical interval of 0.5 m.

obtained from the HYbrid Coordinate Ocean Model (HYCOM) reanalysis. This reanalysis product, with a spatial resolution of 1/12°, assimilates available satellite altimeter observations, *in-situ* SST, and available temperature and salinity profiles from XBTs, Argo floats and moored buoys. The reanalysis has been demonstrated to perform well in reproducing the general features in the China seas (e.g., Jia et al., 2013; Lin et al., 2021). The net heat flux data are downloaded from the National Centers for Environmental Prediction (NCEP) Climate Forecast System Version 2 (CFSv2) (Saha et al., 2010) with a horizontal resolution of 0.5° both in longitude and latitude and hourly time interval.

2.3. Density Ratio and Turner Angle

The density ratio is defined as

$$R \equiv \frac{\alpha \Delta\theta}{\beta \Delta S}, \tag{1}$$

where $\alpha = -\rho^{-1}(\partial\rho/\partial\theta)$ and $\beta = \rho^{-1}(\partial\rho/\partial S)$ are, respectively, coefficients of thermal expansion and saline contraction, $\Delta\theta$ and ΔS are potential temperature and salinity differences taken over a horizontal spatial interval, and ρ the density. Positive values of R mean that temperature and salinity have opposing effect on density while negative R means they have the same effect on density. Regardless of the sign of R, $|R| > 1$ corresponds to T-dominated type of density changes whereas $|R| < 1$ corresponds to S-dominated. As mentioned above, $R = 1$ means exact T-S compensation. There are two limitations of using R to quantify the relative effect of temperature and salinity on density: (a) the range of R could be infinite depending on the values of $\Delta\theta$ and ΔS; (b) when $\Delta S = 0$, R becomes indeterminate. These limitations can be overcome by introducing the Turner angle which is defined as

$$\mathrm{Tu} = \arctan(R). \tag{2}$$

Correspondingly, $\mathrm{Tu} > 0$ ($\mathrm{Tu} < 0$) represents that temperature and salinity are compensated (constructed) with each other; $|\mathrm{Tu}| > \pi/4$ and $-\pi/4 < \mathrm{Tu} < \pi/4$ corresponds to T-dominated and S-dominated density changes, respectively, and $\mathrm{Tu} = \pi/4$ corresponds to exact T-S compensation.

3. Frontal Structure in the Taiwan Strait

In this section we will show the horizontal feature of the front in the Taiwan Strait and its evolution with satellite and reanalysis datasets, and the vertical structure of the front with towed measurements.

3.1. Horizontal Structure

The circulation and thermohaline features in the Taiwan Strait are significantly affected by the Asian monsoon. It is well known that strong northeasterlies prevail from October to next April and southwesterlies dominate from June to August, with May and September being the transitional periods (e.g., Hu et al., 2010). Nevertheless, the onset and cessation of monsoon have been demonstrated to be subject to significant variability on different time scales (e.g., Ding & Chan, 2005), so the beginning and transitional times vary from year to year. For example, the reanalysis indicates that in 2018 northeasterly winds prevailed from September (instead of October) to the next May (instead of April) with significant cessation occurring in April 2019 (Figure 3).

The surface currents in the western Taiwan Strait (i.e., Zhe-Min Coastal Current on the mainland side) are strongly influenced by the prevailing monsoon and hence flow south-southwestward in winter and northeastward in summer. Presumably due to its shallowness, surface currents in this region responded fairly fast to the monsoon with evident south-southwestward flows from October 2018 to March 2019, and the monsoon cessation in April 2019 was also accompanied by rather weak surface currents with no evident directions near the mainland (Figure 3). In May 2019, when the northeasterly winds continued to blow, the coastal current had already reversed to flow northeastward. Surface currents in the central and eastern Taiwan Strait flow northeastward all year around due to the presence of the South China Sea Warm Current and the intruding Kuroshio, and hence they flow upwind in winter (Figure 3).

Accompanied by the seasonal variation of the Zhe-Min Coastal Current, the SST front in the Taiwan Strait evolves accordingly. We mark the location of the front by the 16°C isotherm which roughly outlines the boundary

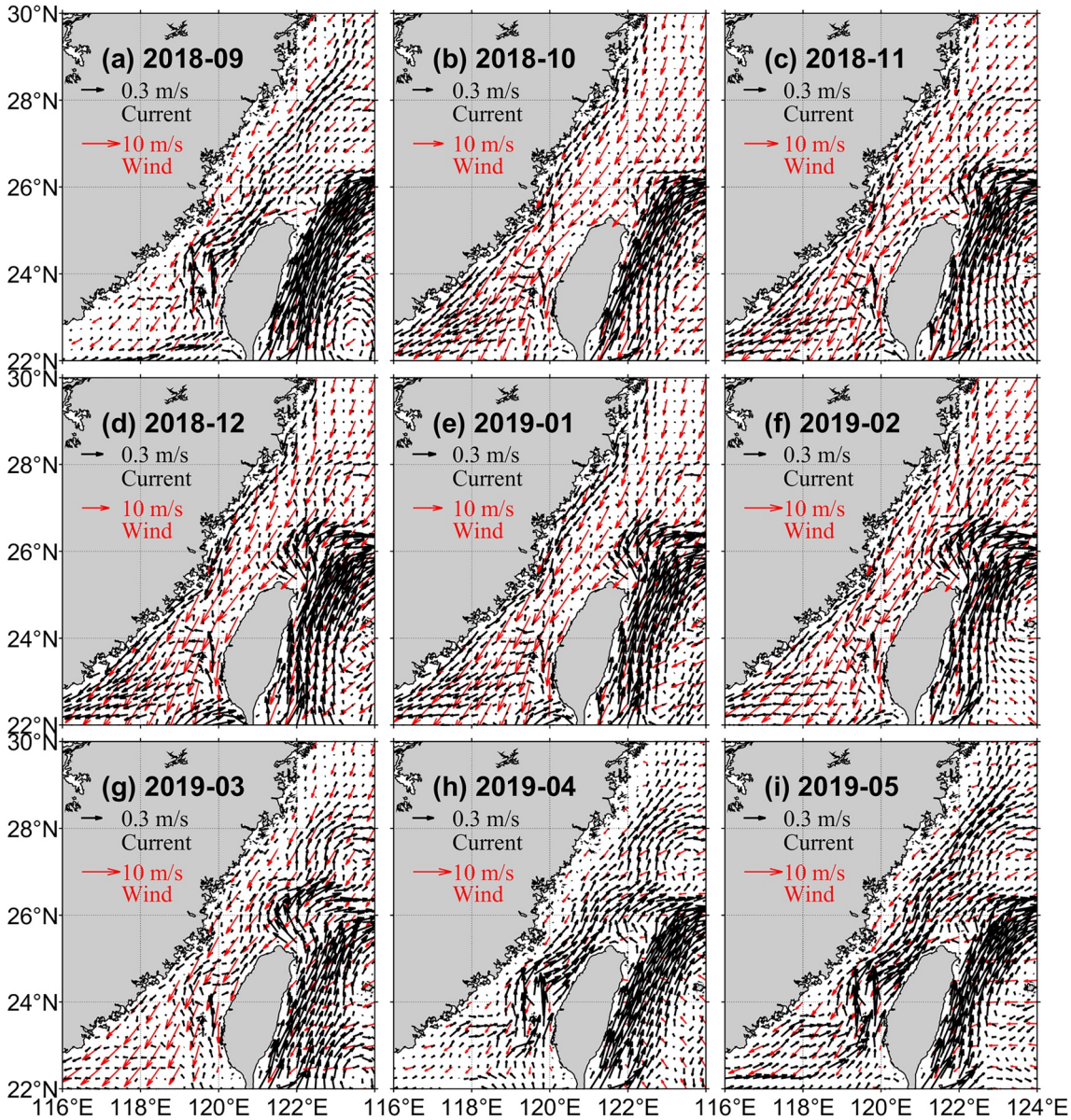

Figure 3. Monthly mean surface ocean currents (black arrows) and winds (red arrows) in the Taiwan Strait from September 2018 to May 2019. The ocean currents are based on HYbrid Coordinate Ocean Model reanalysis and wind data are based on Climate Forecast System Version 2 reanalysis.

of coastal waters (Figure 4). It is shown that prominent SST front started to appear from December 2018, situated north of the Taiwan Strait near the coast (Figure 4b). The SST front became strongest in January and February 2019, with the coastal waters extending southwestward throughout the Strait; although the majority of coastal waters occupied the region on the mainland flank, the outer boundary reached the eastern part of the Strait (Figures 4c and 4d). The SST front weakened in March and got significantly decayed in April as the Zhe-Min Coastal Current retreated (Figures 4e and 4f).

3.2. Vertical Structure

The towed measurements indicate that in the upper 30 m of the Taiwan Strait, there were relatively strong fronts of both temperature and salinity with nearly vertical isotherms and isohalines during the sampling period (Figure 5). Across section CD, the maximum gradients of temperature and salinity exceeded 2°C km^{-1} and 0.5 km^{-1}, respectively. Beneath 30 m depth, the fronts tilted to the shallower region (i.e., mainland side) with increasing depth

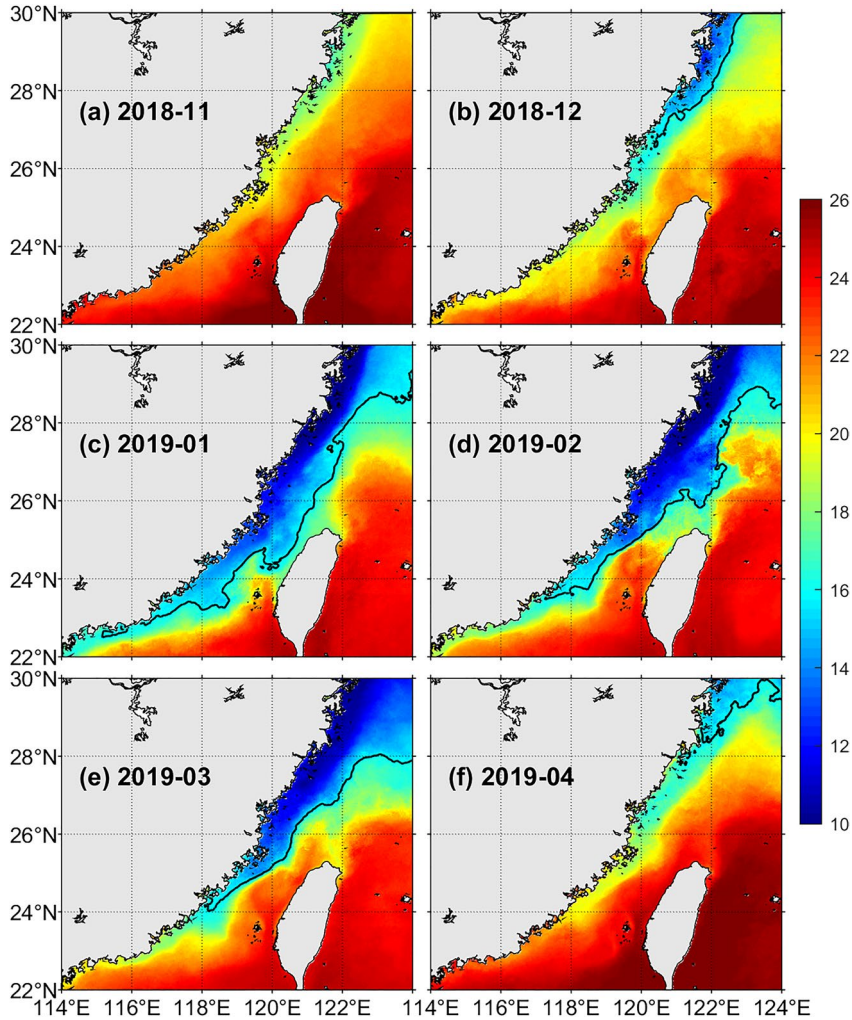

Figure 4. Himawari 8-based monthly mean sea surface temperature (SST) in the Taiwan Strait from November 2018 to April 2019, indicating evolution of the SST front. The thick black curves denote the 16°C isotherm as an indication of the SST front.

and the intensity of the front gradually decreased. In both sections AB and CD, the temperature front was almost co-located with the salinity front (see white solid and vertical black dashed lines in the top and middle panels of Figure 5). Since the temperature and salinity on the two sides of the front had opposing effect on density, density front was absent in the position of temperature or salinity front. Interestingly, the density at the interface (or transition zone) between the coastal and offshore waters appeared to be larger than that at both sides. This seems to suggest the occurrence of cabbeling, referred to a process that two water masses with different temperature and salinity yet the same density would become denser after mixing. This phenomenon is due to the nonlinearity of the equation of state of seawater and is often observed at fronts (Thomas & Shakespeare, 2015). (In the study area, nevertheless, densities on the two sides of the front are not exactly the same, with the offshore water slightly denser than the coastal water.) There seemed to exist two density fronts: one between the coastal water and the transition zone and the other weaker one between the transition zone and the offshore water (see white solid lines in the bottom panels of Figure 5). The western density front at section CD is the strongest among the observed ones, with an intensity of 0.2 kg m^{-3} km^{-1}. The isopycnals at the two density fronts tilted apart with increasing depth, forming a cone-shaped structure (bottom panels of Figure 5).

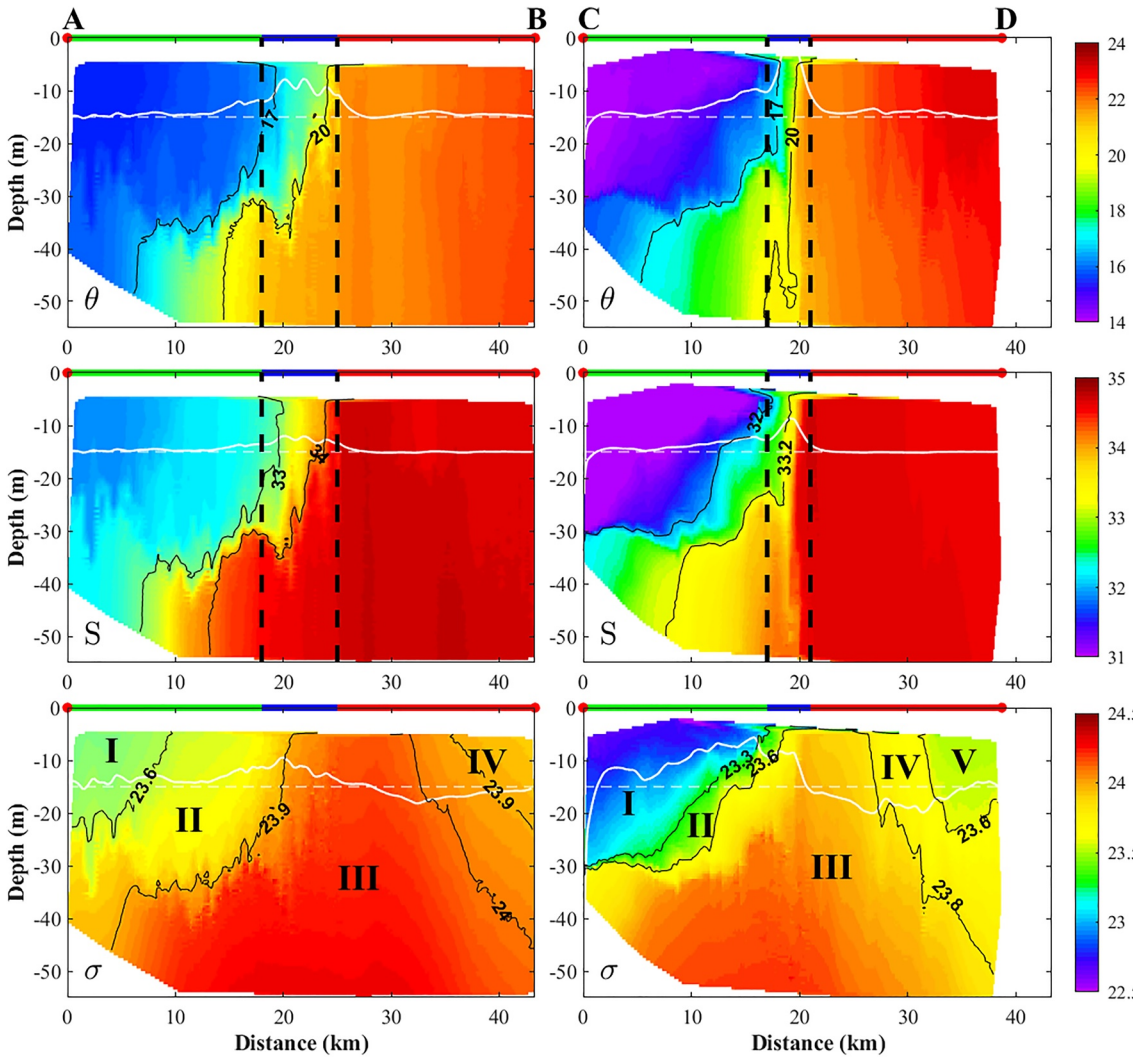

Figure 5. Sectional distribution of the (top) potential temperature (θ in °C), (middle) salinity (S) and (bottom) potential density (σ in kg m^{-3}) across sections (left) AB and (right) CD. White dashed lines denote the 15-m depth and the white solid lines denote the horizontal gradients of the corresponding variables at this depth. The vertical black dashed lines denote the position of the T/S front. The green, blue and red bars on the top axes represent the regions west of the temperature front, across the front and east of the front, respectively. The Roman numerals in the bottom panels denote regions partitioned by isopycnals.

4. T-S Compensation in Frontal Regions of the Taiwan Strait

We now examine the T-S compensation across the frontal regions in the Taiwan Strait. In particular, we explore the scale dependence of the compensation for waters of different origins, and seek to reveal the underlying mechanism.

4.1. Overall Compensation Across the Front

We first plot the magnitude of $\alpha\Delta\theta$ and $\beta\Delta S$ across sections AB and CD, and it confirms co-location of the temperature and salinity fronts (top and middle panels of Figure 6), as indicated by Figure 5. Moreover, $|\beta\Delta S|$ is slightly larger than $|\alpha\Delta\theta|$ to the west of the front for both sections AB and CD, while the opposite occurs to the east of the front although both $|\alpha\Delta\theta|$ and $|\beta\Delta S|$ are much weaker compared to their counterparts west of the front; within the frontal area, $|\alpha\Delta\theta|$ and $|\beta\Delta S|$ are comparable. Given such sectional distributions of $|\alpha\Delta\theta|$ and $|\beta\Delta S|$, it is expected to have $|\mathrm{Tu}| < \pi/4$ to the west of the front, suggesting an S-dominated density change on the mainland side, $|\mathrm{Tu}| > \pi/4$ to the east of the front, suggesting a T-dominated density change in the central strait, and $|\mathrm{Tu}| \approx \pi/4$ within the frontal area, suggesting a roughly exact T-S compensation in the transition zone. These are all consistent with the sectional distribution of Tu (bottom panels of Figure 6).

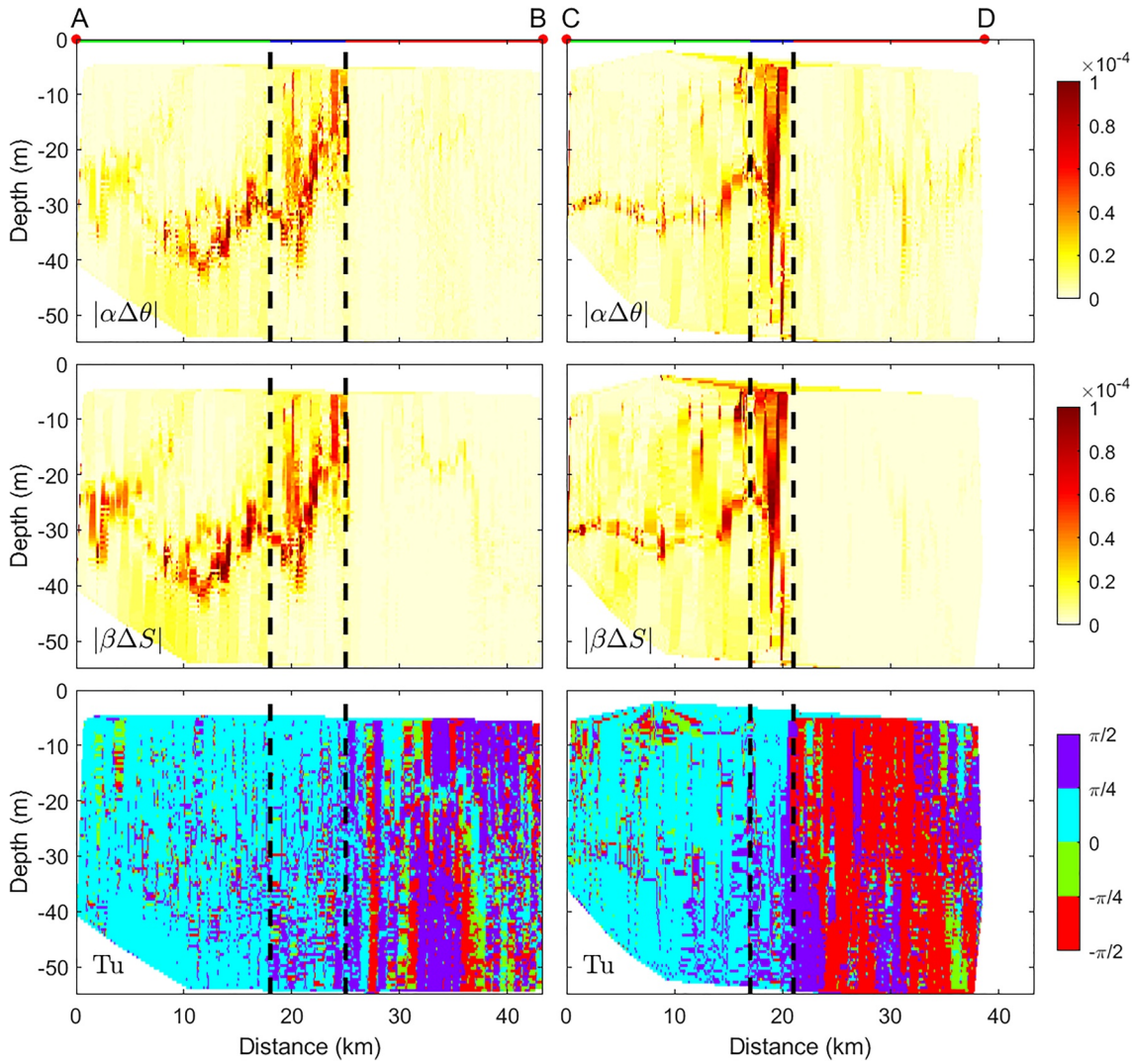

Figure 6. Sectional distribution of (top) $|\alpha\Delta\theta|$, (middle) $|\beta\Delta S|$ and (bottom) the Turner angle (Tu) across sections (left) AB and (right) CD. Both $\alpha\Delta\theta$ and $\beta\Delta S$ are in kg m^{-3}. The vertical black dashed lines are the same as in Figure 5 denoting the position of the T/S front.

Given the patchiness in the sectional distribution of Tu, we further examine the T-S compensation using the probability density functions (PDFs) of Turner angle in different partitioned areas. We first divide the cross-frontal sections into three regions according to the location of the T/S front (defined by the vertical black dashed lines in Figures 5 and 6). The PDFs of Tu indicate that waters to the west of the T/S front mostly had $0 < \mathrm{Tu} < \pi/4$, suggesting an S-dominated type of density variations, which are partially compensated by temperature variability (green lines in Figures 7a and 7b). In the frontal region, the peak of Tu PDFs is close to $\pi/4$ suggesting a nearly exact T-S compensation (blue lines in Figures 7a and 7b). This is why density front is not seen in the location of the T/S front (Figure 5). To the east of the T/S front, $|\mathrm{Tu}| > \pi/4$ suggests a T-dominated type but salinity changes could either compensate or construct the effect of temperature changes on density (red lines in Figures 7a and 7b). Such T-S compensating characteristics are consistent with our expectations given the origins of the confluent waters that form the front in the central Taiwan Strait. As mentioned above, there is a density front on each side of the T/S front. We are then able to identify an S-dominated density front and a T-dominated density front, which will be used for further analysis of the scale dependence of compensation detailed in the next subsection.

Different from the nearly vertical T/S fronts, the density fronts are slanted in both sections AB and CD. Hence the above region partition based on the T/S front may have included waters of different origins, in particular for waters below 30-m depth. We thus divide regions according to the isopycnals and then re-calculate the PDFs of

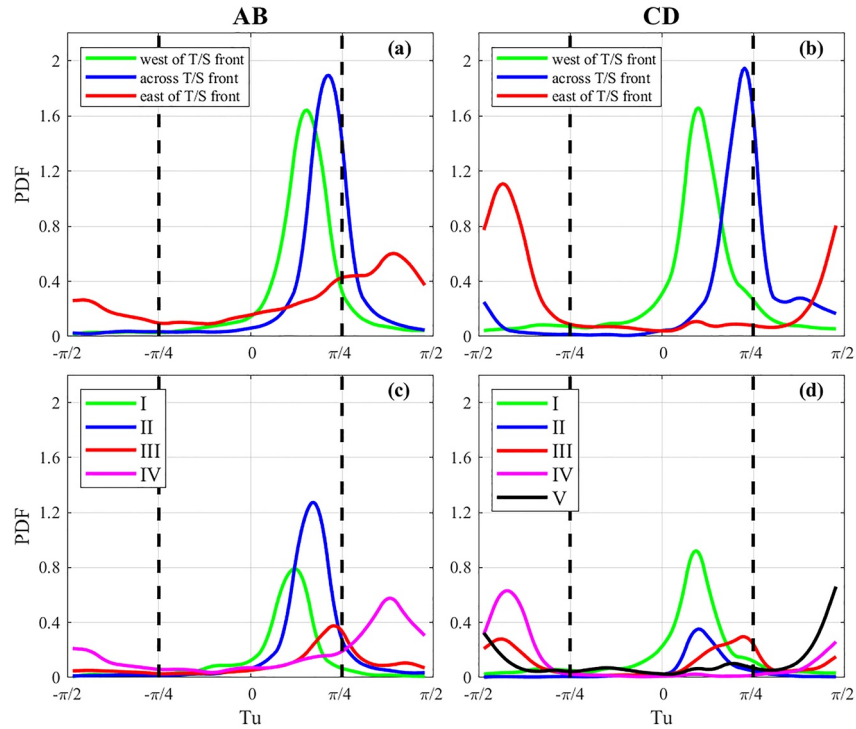

Figure 7. Probability density functions of Turner angle for partitioned regions based on (upper) the T/S front and (lower) isopycnals in sections (left) AB and (right) CD. Calculations are based on data from the upper 30 m. The colors of the lines correspond to different partitioned regions labeled in the legend in each panel. The Roman numerals in the lower panels correspond to the regions in the bottom panels of Figure 5.

Turner angle. For the western density front and the region west of it (Zones I and II in Figure 5), it is S-dominated with temperature changes partially opposing salinity effect on density (green and blue lines in Figures 7c and 7d). For the eastern density front and the region east of it (Zones IV and V in Figure 5), it is T-dominated type of density changes (magenta and black lines in Figures 7c and 7d). For the transition zone between the two density fronts (Zone III in Figure 5), Tu $\approx \pi/4$ suggesting a nearly exact T-S compensation (red lines in Figures 7c and 7d), which is also evidenced by the weak density gradients in this region. These are consistent with the results based on the region partition according to the T/S front. For convenience, we will use the previous partition scheme based on the T/S front to identify the western S-dominated density front and the eastern T-dominated density front.

4.2. Scale Dependence of the Frontal Compensation

We now examine the scale dependence of the compensation for the S-dominated and T-dominated density fronts (subsections marked by the green and red top bars in Figure 5, respectively). Considering the spatial sampling resolution and length of the sections, we bandpass filter the entire section to obtain $\alpha\Delta\theta$ and $\beta\Delta S$ series with scales of 1 and 10 km, and the (scale-dependent) Turner angle is then calculated using the filtered $\alpha\Delta\theta$ and $\beta\Delta S$ data. (The filtering cutoff wavelengths are 0.5 and 2 km for the 1-km scale, and 5 and 20 km for the 10-km scale, respectively.) The Tu values at the S-dominated and T-dominated density fronts are subsequently obtained by partitioning the filtered Tu in the entire section into regions west of the front and east of the front.

For the region west of the T/S front, the PDFs of Turner angle for both the O(1 km) and O(10 km) scales reveal S-dominated type for both sections AB and CD (gray lines in the upper two rows of panels of Figure 8), consistent with the above calculations based on the original data (Figure 7). Closer inspection of Figure 8 suggests that temperature variability opposes the effect of salinity variability on density to a larger extent at O(1 km) scale than at O(10 km) scale. This is shown more clearly in the histograms of density ratios calculated using the largest 5% values of $\alpha\Delta\theta$ and $\beta\Delta S$ (green bars in Figure 8): Tu $= \pi/4$ is more frequently observed at the O(1 km) scale. In other words, temperature and salinity are more compensated with decreasing spatial scale in the

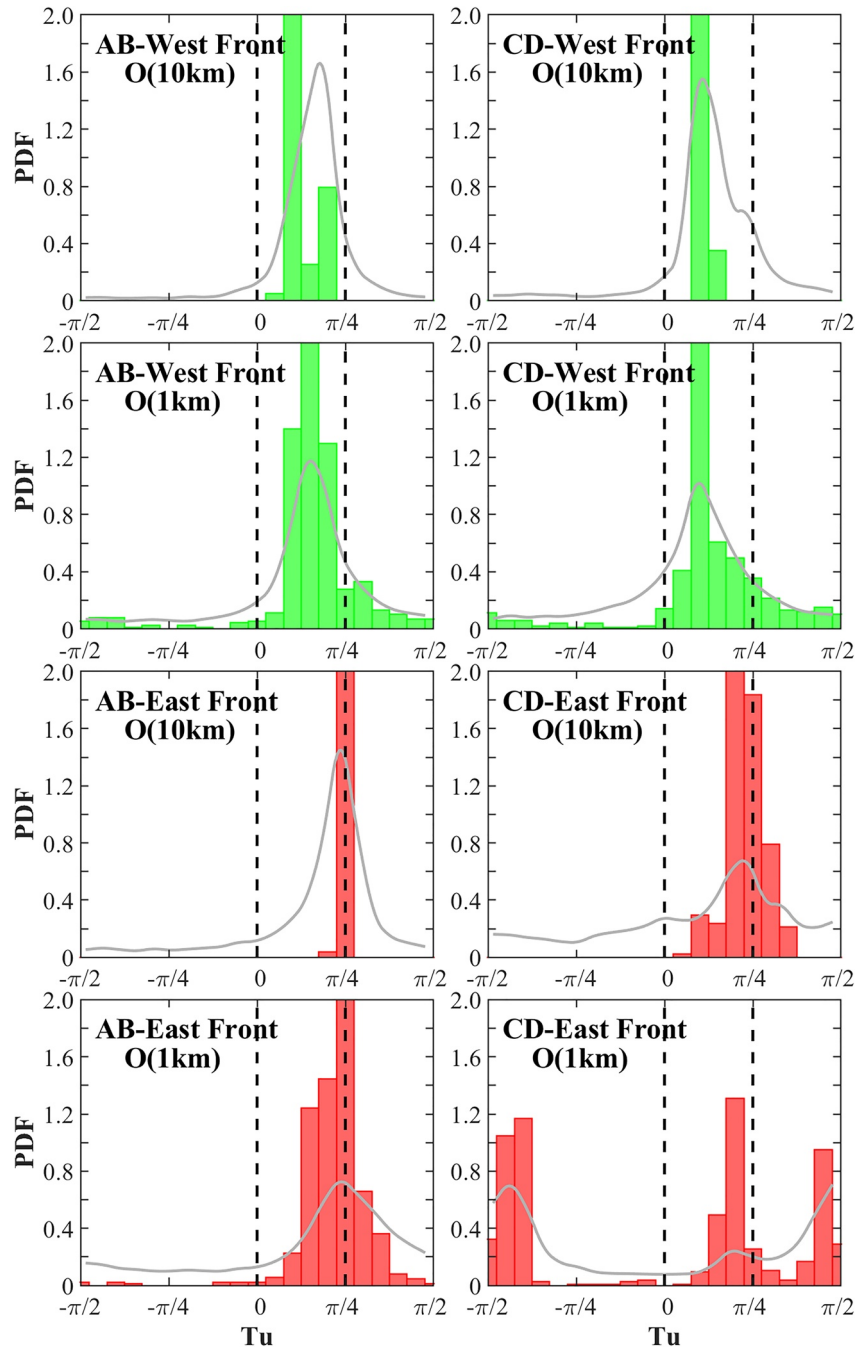

Figure 8. Probability density functions (gray lines) of Turner angle at O(1 km) and O(10 km) scales for regions west of the temperature front (upper two rows of panels) and east of the front (lower two rows of panels) in sections AB (left) and CD (right). The green and red bars denote histograms of density ratios calculated using the largest 5% values of $\alpha\Delta\theta$ and $\beta\Delta S$ in each panel.

S-dominated density frontal region. This is consistent with the finding of the submesoscale-selective compensation by Spiro Jaeger and Mahadevan (2018) in the S-dominated Bay of Bengal.

For the region east of the T/S front, the PDFs of Turner angle show almost exact T-S compensation at O(10 km) scale (the third row of panels of Figure 8), in particular for the eastern subsection of AB since the density gradients are rather weak there (Figure 5). The histograms of the top 5% density ratios are almost all concentrated on Tu $= \pi/4$. At O(1 km) scale, however, the degree of compensation is obviously reduced (bottom panels of Figure 8), in particular for section CD. There is still a considerable portion of exact compensation in the eastern

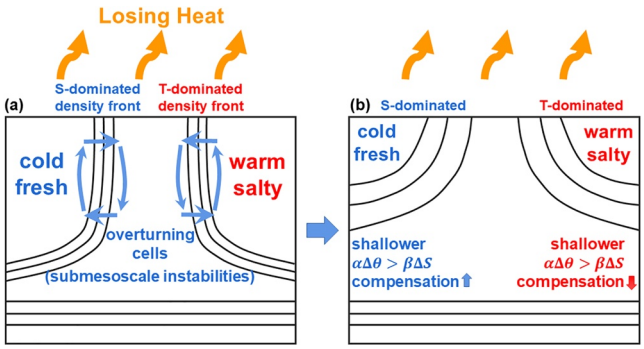

Figure 9. Schematic illustrating mechanisms by which heat flux and restratification lead to the contrasting scale dependence of compensation in the S-dominated and T-dominated frontal regions. See the main texts for details.

subsection of AB at O(1 km) scale, but the departure from exact compensation is evident. We thus observe an interesting phenomenon, namely, *temperature and salinity are less compensated with decreasing spatial scale in the T-dominated density frontal region*. This is in great contrast to the finding in the S-dominated region, and seems to have not been documented before. We will explore the mechanisms of this phenomenon in the next section.

It is also interesting to note that the O(1 km) Turner angle PDFs for the eastern fronts (bottom panels of Figure 8) indicate S-dominated submesoscale fronts at section AB but T-dominated ones at section CD; we suspect this contrasting feature might be related to the strength and extent of the warm current in the central Taiwan Strait, but definitive physical reasons are yet to be constrained and require more towed measurements to the east of the front.

4.3. Mechanisms

Strong fronts tend to slump due to gravity inducing overturning cells that push the isopycnals from vertical toward horizontal (Rudnick & Ferrari, 1999), and converting the potential energy stored in the fronts to kinetic energy of corresponding flows (Figure 9a). This restratification process is accompanied by submesoscale instabilities aroused in the mixed layer and hence is indicative of the generation of submesoscale motions (McWilliams, 2016). Since two density fronts are formed in the Taiwan Strait when the coastal colder and fresher water interfaces with the offshore warmer and saltier water, the overturning cells at the two density fronts would result in convergent flows in the surface transition zone and downwelling in the mixed layer (Figure 9a). This would thus result in slanted, cone-shaped isopycnals (Figure 9b) as observed from the towed measurements (bottom panels of Figure 5).

To further verify the above hypothesis, we need to check whether submesoscale motions were indeed active in the frontal regions. Based on underway velocity measurements, we calculate the wavenumber spectra of horizontal kinetic energy for all cross-frontal sections (black dashed lines in Figure 1) and then obtain a mean wavenumber spectrum for the upper 30 m. The mean spectrum closely follows the k^{-2} scaling (k being the along-track wavenumber) in the resolved submesoscale range (Figure 10), indicating active submesoscale motions in the sampled region (e.g., Capet et al., 2008). This provides evidence for the occurrence of submesoscale instabilities in the frontal mixed layer. The generation mechanisms of submesoscale motions include mixed-layer instability (MLI), strain-induced frontogenesis, turbulent thermal wind (TTW) mechanism, etc (McWilliams, 2016). MLI is basically baroclinic instability in the mixed layer (Boccaletti et al., 2007); TTW balance is a synthesis of geostrophic, hydrostatic and Ekman-layer dynamics, taking vertical viscosity in boundary layers into account (McWilliams, 2017). Both MLI and TTW can induce submesoscale restratification as illustrated in Figure 9, but given the relatively strong winter monsoon in the Taiwan Strait and its shallowness, it is possible that TTW plays an important role in the generation of submesoscale instabilities and the regulation of restratification process in the study region. But to obtain definitive mechanisms would require more in-depth investigations such as diagnostic or sensitivity analyses based on numerical simulations that could generally reproduce the phenomena observed here.

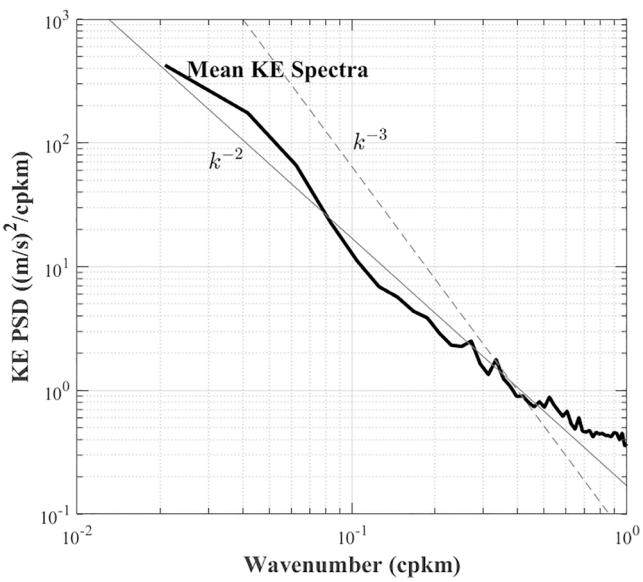

Figure 10. Mean wavenumber spectrum of horizontal kinetic energy (heavy black curve) for all cross-frontal sections (black dashed lines in the right panel of Figure 1) using the upper 30-m velocities collected by a shipboard underway ADCP. The thin gray solid and dashed lines denote the spectral slopes of k^{-2} and k^{-3}, respectively.

We now explore mechanisms of the contrasting scale dependence of the T-S compensation in the S-dominated and T-dominated frontal regions (Figure 8). As illustrated in Figure 9, the submesoscale instability-induced overturning cells increased the stratification on both sides of the transition zone, and rendered the mixed layer to become shallower on both sides.

For the western density front that was originally S-dominated, if a surface cooling (i.e., upward net heat flux) occurs in the frontal region, the shallower mixed layer on the coastal flank of the western density front would experience a larger temperature drop. This would naturally increase the degree

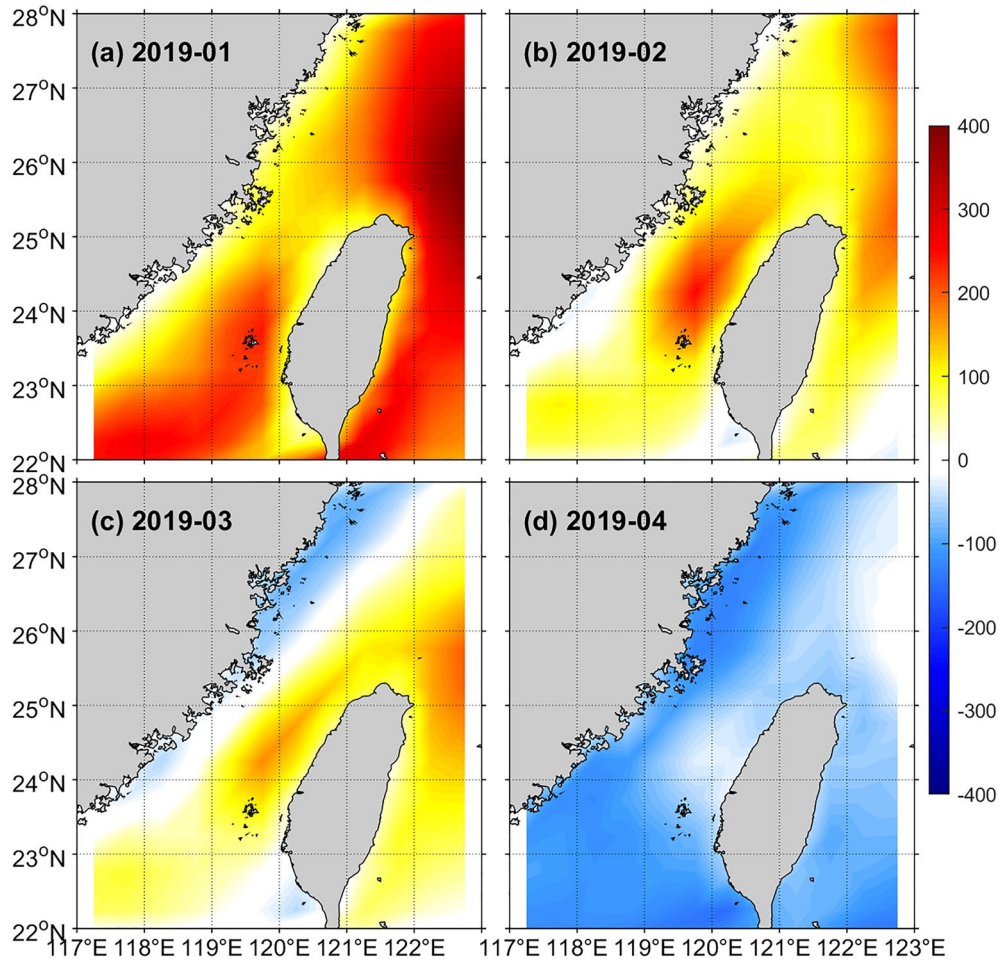

Figure 11. Monthly mean net heat flux (in W m^{-2}) around the Taiwan Strait from January to April 2019 based on the National Centers for Environmental Prediction Climate Forecast System Version 2 reanalysis. Positive values indicate heat loss from the ocean to the atmosphere.

of T-S compensation at the scale for submesoscale instabilities to develop (i.e., O(1 km)), consistent with the increasing compensation with decreasing spatial scale (Figure 8). This hypothetical process is in accord with that proposed by Spiro Jaeger and Mahadevan (2018) for the S-dominated Bay of Bengal.

For the eastern density front, although the scale dependence of T-S compensation is opposite to that in the S-dominated density front (i.e., decreasing compensation with decreasing scale), the restratification-cooling mechanism can also work here. The restratified eastern density front had shallower mixed layer on the offshore flank, which should have responded with a larger temperature reduction to surface cooling. The consequence is that the degree of T-S compensation decreased for the originally T-dominated type of density changes, also consistent with that shown in Figure 8.

The above restratification-cooling mechanism assumes a surface cooling occurring at the frontal regions. The question is whether this was truly happening in the spring of 2019 when the field measurements were conducted. We now check this using the NCEP CFSv2 reanalysis. As shown in Figure 11, the monthly averages clearly indicate positive (i.e., upward) net heat flux around the Taiwan Strait from January to March 2019, indicating that the frontal region indeed experienced surface cooling during our field measurements and the period prior to it. The upward heat flux seemed to have a decreasing trend from January to March and reversed its sign in April, but this does not violate our assumption mentioned above and the frontal structure had become rather weak in April anyway (Figure 4).

5. Summary and Discussion

Based on a combination of high-resolution in situ measurements, satellite and reanalysis products, the present study investigates the frontal structure in the Taiwan Strait and T-S compensation in frontal regions. One of our key findings is the contrasting scale dependence of the density compensation in the S-dominated and T-dominated frontal areas.

The satellite images reveal that an SST front appeared in the Taiwan Strait from December 2018, got intensified in January and February 2019 and significantly weakened in April. This front was formed as the cold and fresh waters carried by the Zhe-Min Coastal Current encountered the warm and salty waters carried by the extended South China Sea Warm Current. The cross-frontal towed measurements indicate that the temperature front and salinity front were almost co-located with a relatively strong intensity. Due to T-S compensation, density front was absent in the location of temperature/salinity front, replaced by a transition zone with the largest density but weak gradients. Interestingly, two slanted density fronts were generated with the transition zone saddled in between, forming a cone-shaped isopycnal distribution in the cross-frontal section.

The analyses based on density ratio and Turner angle suggest S-dominated and T-dominated types of density changes in the western and eastern density fronts, respectively. This is expected as the Zhe-Min Coastal Current is strongly influenced by the river runoff and salinity changes naturally dominated, whereas the warm and salty waters originated from the deep ocean and the effect of salinity variations on density is supposed to be smaller than that induced by temperature variations. Within the transition zone, exact T-S compensation was observed, which explains why no density front was seen.

Scale dependence of T-S compensation is further examined in the two density frontal regions. Temperature and salinity are more compensated from O(10 km) to O(1 km) scale in the S-dominated frontal region, consistent with previous findings in the Bay of Bengal. Interestingly, temperature and salinity are found to be less compensated from O(10 km) to O(1 km) scale in the T-dominated frontal region. In fact, the contrasting compensating characteristics can be both interpreted by the submesoscale restratification-cooling mechanism. Specifically, the overturning cells induced by submesoscale instabilities slump isopycnals in the frontal area from vertical to horizontal, shoaling the mixed layer on the coastal flank of the western density front and on the offshore flank of the eastern density front. When the sea surface experiences upward net heat flux, larger temperature drops would occur in the shallower mixed layers. This would thus increase (decrease) the degree of T-S compensation in the S-dominated (T-dominated) frontal region at the scale for submesoscale instabilities to develop, that is, O(1 km).

Whether findings in the present study are generic requires further investigation on certain aspects. First, due to practical reasons, all the sampled cross-frontal sections have a length shorter than 50 km, which only marginally resolve the O(10 km) scale and are not able to resolve larger scales at mesoscale. Therefore, whether the scale dependence of density compensation continues to hold at larger scales needs further studies based on measurements over longer sections. Second, we propose that the restratification-cooling mechanism could explain the submesoscale-selective compensation in both the S-dominated and T-dominated fronts. In a broader context, we are interested in whether the proposed mechanism is generic or only applied to the particular setting of fronts formed by confluent waters with compensated temperature and salinity. Even if it is the latter, it is also worthwhile to check whether the mechanism applied to larger-scale fronts in the world oceans, for example, the prominent fronts often observed in the western boundary current extensions. In particular, does the conclusion of decreasing degree of compensation with decreasing spatial scale in T-dominated fronts also hold in the open ocean (as most open-ocean waters are T-dominated)? Dedicated process-oriented observations over longer sections that traverse particular thermohaline regimes are needed to disclose the above queries, which will help understand the broader impact of the proposed restratification-cooling mechanism.

Data Availability Statement

The towed measurements used to generate figures in this study could be obtained from https://osf.io/dk83v/. The Himawari 8 SST product is obtained from the Japan Aerospace Exploration Agency (https://global.jaxa.jp/). The mean surface ocean currents are obtained from the HYCOM reanalysis (https://www.hycom.org/data/glbu0pt08/expt-19pt0). The net heat flux data are downloaded from NCEP CFSv2 (https://rda.ucar.edu/datasets/ds094.1/).

Acknowledgments
This work was supported by the National Natural Science Foundation of China (Grants 42076013, 91958203, 91858201, 41890801, 41730533). The authors thank Chuanyin Wang, Zhendong Hu, Xue Sun and the crew of R/V Yanping 2 for the help in the data collection during the cruise and data processing and discussion after the cruise. We appreciate the Editor and three anonymous reviewers who provided insightful comments that have helped improve an early version of the manuscript.

References

Boccaletti, G., Ferrari, R., & Fox-Kemper, B. (2007). Mixed layer instabilities and restratification. *Journal of Physical Oceanography*, *37*(9), 2228–2250. https://doi.org/10.1175/jpo3101.1

Capet, X., McWilliams, J., Molemaker, M., & Shchepetkin, A. (2008). Mesoscale to submesoscale transition in the California current system. Part I: Flow structure, eddy flux and observational tests. *Journal of Physical Oceanography*, *38*(1), 29–43. https://doi.org/10.1175/2007jpo3671.1

Ding, Y., & Chan, J. C. L. (2005). The East Asian summer monsoon: An overview. *Meteorology and Atmospheric Physics*, *89*(1–4), 117–142. https://doi.org/10.1007/s00703-005-0125-z

Ferrari, R., & Rudnick, D. L. (2000). Thermohaline variability in the upper ocean. *Journal of Geophysical Research*, *105*(C7), 16857–16883. https://doi.org/10.1029/2000jc900057

Hu, J., Kawamura, H., Li, C., Hong, H., & Jiang, Y. (2010). Review on current and seawater volume transport through the Taiwan Strait. *Journal of Oceanography*, *66*(5), 591–610. https://doi.org/10.1007/s10872-010-0049-1

Jia, Y., Zhang, Y., & Lin, M. (2013). The numerical simulation of the Kuroshio frontal eddies in the East China Sea using a hybrid coordinate ocean mode. *Acta Oceanologica Sinica*, *32*(5), 31–41. https://doi.org/10.1007/s13131-013-0311-7

Lin, W., Lin, H., & Hu, J. (2021). The tilt of mean dynamic topography and its seasonality along the coast of the Chinese Mainland. *Journal of Geophysical Research: Oceans*, *126*(2), e2020JC016778. https://doi.org/10.1029/2020JC016778

McWilliams, J. C. (2016). Submesoscale currents in the ocean. *Proceedings of the Royal Society A: Mathematical, Physical and Engineering Sciences*, *472*(2189), 20160117. https://doi.org/10.1098/rspa.2016.0117

McWilliams, J. C. (2017). Submesoscale surface fronts and filaments: Secondary circulation, buoyancy flux, and frontogenesis. *Journal of Fluid Mechanics*, *823*, 391–432. https://doi.org/10.1017/jfm.2017.294

Roden, G. I. (1975). On North Pacific temperature, salinity, sound velocity and density fronts and their relation to the wind and energy flux fields. *Journal of Physical Oceanography*, *5*(4), 557–571. https://doi.org/10.1175/1520-0485(1975)005<0557:onptss>2.0.co;2

Rudnick, D. L., & Ferrari, R. (1999). Compensation of horizontal temperature and salinity gradients in the ocean mixed layer. *Science*, *283*(5401), 526–529. https://doi.org/10.1126/science.283.5401.526

Rudnick, D. L., & Martin, J. P. (2002). On the horizontal density ratio in the upper ocean. *Dynamics of Atmospheres and Oceans*, *36*(1–3), 3–21. https://doi.org/10.1016/s0377-0265(02)00022-2

Saha, S., Moorthi, S., Pan, H. L., Wu, X., Wang, J., Nadiga, S., et al. (2010). The NCEP climate forecast system reanalysis. *Bulletin of the American Meteorological Society*, *91*(8), 1015–1058. https://doi.org/10.1175/2010bams3001.1

Spiro Jaeger, G., & Mahadevan, A. (2018). Submesoscale-selective compensation of fronts in a salinity-stratified ocean. *Science Advances*, *4*(2), e1701504. https://doi.org/10.1126/sciadv.1701504

Thomas, L. N., & Shakespeare, C. J. (2015). A new mechanism for mode water formation involving cabbeling and frontogenetic strain at thermohaline fronts. *Journal of Physical Oceanography*, *45*(9), 2444–2456. https://doi.org/10.1175/jpo-d-15-0007.1

Timmermans, M.-L., & Winsor, P. (2013). Scales of horizontal density structure in the Chukchi Sea surface layer. *Continental Shelf Research*, *52*, 39–45. https://doi.org/10.1016/j.csr.2012.10.015